

Properties of the First-order Fermi acceleration in fast magnetic reconnection driven by turbulence in collisional MHD flows

Maria V. del Valle,^{1*} E. M. de Gouveia Dal Pino,^{2†} and G. Kowal^{3,4}

¹*Instituto Argentino de Radioastronomía (IAR), Camino General Belgrano Km 40, Argentina*

²*Instituto de Astronomia, Geofísica e Ciências Atmosféricas, Universidade de São Paulo, Rua do Matão 1226, 05508-900, São Paulo, Brazil*

³*Núcleo de Astrofísica Teórica, Universidade Cruzeiro do Sul, Rua Galvão Bueno 868, 01506-000, São Paulo, Brazil*

⁴*Escola de Artes, Ciências e Humanidades, Universidade de São Paulo, Rua Arlindo Bettio 1000, 03828-000, São Paulo, Brazil*

12 August 2018

ABSTRACT

Fast magnetic reconnection may occur in different astrophysical sources, producing flare-like emission and particle acceleration. Currently, this process is being studied as an efficient mechanism to accelerate particles via a first-order Fermi process. In this work we analyse the acceleration rate and the energy distribution of test particles injected in three-dimensional magnetohydrodynamical (MHD) domains with large-scale current sheets where reconnection is made fast by the presence of turbulence. We study the dependence of the particle acceleration time with the relevant parameters of the embedded turbulence, i.e., the Alfvén speed V_A , the injection power P_{inj} and scale k_{inj} ($k_{inj} = 1/l_{inj}$). We find that the acceleration time follows a power-law dependence with the particle kinetic energy: $t_{acc} \propto E^\alpha$, with $0.2 < \alpha < 0.6$ for a vast range of values of $c/V_A \sim 20 - 1000$. The acceleration time decreases with the Alfvén speed (and therefore with the reconnection velocity) as expected, having an approximate dependence $t_{acc} \propto (V_A/c)^{-\kappa}$, with $\kappa \sim 2.1 - 2.4$ for particles reaching kinetic energies between $1 - 100 m_p c^2$, respectively. Furthermore, we find that the acceleration time is only weakly dependent on the P_{inj} and l_{inj} parameters of the turbulence. The particle spectrum develops a high-energy tail which can be fitted by a hard power-law already in the early times of the acceleration, in consistency with the results of kinetic studies of particle acceleration by magnetic reconnection in collisionless plasmas.

Key words: acceleration of particles — magnetic reconnection — magnetohydrodynamics — methods: numerical

1 INTRODUCTION

Magnetic reconnection occurs when two magnetic fluxes of opposite polarity encounter each other. Under finite magnetic resistivity conditions a current sheet is formed at the discontinuity surface, where the field lines annihilate. Direct evidence of magnetic reconnection in astrophysical and space environments like the solar corona and the Earth magnetotail indicate that in some circumstances reconnection can be very fast, with rates which are a substantial fraction of the Alfvén speed V_A .

Fast reconnection breaks the magnetic field topology releasing magnetic energy explosively thus explaining the bursty emission, for instance, in solar flares.

Relativistic particles are always observed in connection with these flares suggesting that magnetic reconnection can lead to direct particle acceleration (see e.g., the reviews [de Gouveia Dal Pino, Kowal, & Lazarian 2014](#); [de Gouveia Dal Pino & Kowal 2015](#); [Uzdensky 2011](#), and references therein).

In analogy to diffusive shock acceleration (DSA), in which particles confined between the upstream and downstream flows undergo a first-order Fermi acceleration, [de Gouveia dal Pino & Lazarian \(2005\)](#) (hereafter GL05) proposed a similar process occurring within the current sheet where trapped particles bounce back and forth between the converging magnetic fluxes of opposite polarity in the large-scale reconnection region. The particles gyrorotate around a reconnected magnetic field (see Figure 2b in [Kowal, de Gouveia Dal Pino, & Lazarian](#)

* E-mail: maria@iar-conicet.gov.ar (MVdV)

† E-mail: dalpino@iag.usp.br (EMGDP)

2011), gaining energy due to collisions with magnetic irregularities at a rate $\Delta E/E \propto V_{\text{rec}}/c$ (where V_{rec} is the reconnection speed) implying a first-order Fermi process with an exponential energy growth after several round trips (GL05, de Gouveia Dal Pino & Kowal 2015). A similar process was also invoked by Drake et al. (2006) who investigated particles accelerated inside two-dimensional contracting magnetic islands (or loops). In Kowal, de Gouveia Dal Pino, & Lazarian (2011) it has been demonstrated the equivalence between the two mechanisms for driving first-order Fermi acceleration. This process has been extensively tested numerically mainly through two-dimensional (2D) particle-in-cell (PIC) simulations of collisionless electron-ion or electron-positron plasmas (e.g., Drake et al. 2006; Zenitani & Hoshino 2001, 2007, 2008; Lyubarsky & Liverts 2008; Drake et al. 2010; Clausen-Brown & Lyutikov 2012; Cerutti et al. 2014; Li et al. 2015), and more recently also through three-dimensional (3D) PIC simulations (Sironi & Spitkovsky 2014; Guo et al. 2015, 2016). However, these simulations can probe acceleration only at the kinetic scales of the plasma, of a few hundreds of the inertial length ($\sim 100c/\omega_p$, where ω_p is the plasma frequency). To assess the first-order Fermi process in the large scales of the collisional MHD flows commonly observed in astrophysical systems, Kowal, de Gouveia Dal Pino, & Lazarian (2011, 2012) have also successfully tested it in 2D and 3D MHD simulations injecting test particles in the reconnection domain.

Currently, fast magnetic reconnection is regarded as a potentially important mechanism to accelerate particles not only in the solar system context (e.g., Drake et al. 2006, 2009; Gordovskyy, Browning, & Vekstein 2010; Gordovskyy & Browning 2011; Zharkova et al. 2011; Lazarian & Opher 2009; Drake et al. 2010; Lazarian & Desiati 2010; Li et al. 2015), but also beyond it, in galactic and extragalactic environments such as jet-accretion disk systems (e.g., de Gouveia dal Pino & Lazarian 2005; de Gouveia Dal Pino, Piovezan, & Kadowaki 2010; de Gouveia Dal Pino et al. 2010; Giannios 2010; del Valle et al. 2011; Kadowaki, de Gouveia Dal Pino, & Singh 2015; Khiali, de Gouveia Dal Pino, & del Valle 2015; Khiali, de Gouveia Dal Pino, & Sol 2015), pulsar winds and GRBs (e.g., Lazarian et al. 2003; Zenitani & Hoshino 2007; Zhang & Yan 2011; Uzdensky 2011; Clausen-Brown & Lyutikov 2012; Cerutti et al. 2014; Sironi & Spitkovsky 2014; Guo et al. 2014, 2015; Singh, Mizuno, & de Gouveia Dal Pino 2016). It has been also related to the production of ultra-high-energy cosmic rays (e.g., de Gouveia Dal Pino & Lazarian 2000, 2001; Kotera & Olinto 2011). Besides, the accelerated particles may produce detectable non-thermal emission in a wide range of energies, specially at gamma rays (e.g., del Valle et al. 2011; Vieyro & Romero 2012; Cerutti et al. 2014; Khiali, de Gouveia Dal Pino, & del Valle 2015; Khiali, de Gouveia Dal Pino, & Sol 2015; Kadowaki, de Gouveia Dal Pino, & Singh 2015; Singh, de Gouveia Dal Pino, & Kadowaki 2015) or neutrinos (e.g., Khiali & de Gouveia Dal Pino 2016), therefore, studies of the acceleration rate and the particle power-law

index are fundamental for understanding and modelling this emission.

As remarked above, in order to obtain an efficient acceleration process, reconnection has to be fast. In collisionless plasmas, this is usually ensured by kinetic instabilities or by the Hall effect (in the case of an electron plasma), both relevant only at plasma kinetic scales. In large-scale collisional MHD systems, fast reconnection can be driven either by anomalous resistivity (Parker 1979; Biskamp 1997; Zenitani, Hesse, & Klimas 2009) or by turbulence (Lazarian & Vishniac 1999; Kowal et al. 2009, 2012; Lazarian et al. 2012)¹.

In a weak turbulent medium, the wandering of the magnetic field lines allows for many simultaneous events of reconnection to happen at the same time. Moreover, the reconnected flux is more efficiently removed due to turbulence which broadens the outflow channel (see Figure 1 in Kowal et al. 2009, for example). These two factors make such reconnection fast. According to Lazarian & Vishniac (1999), $V_{\text{rec}} \sim V_A(l/L)^{1/2}(v_l/V_A)^2$, where v_l and l are the injection velocity and scale of the turbulence, respectively. It is easy to see that for the upper limit, i.e. $l \sim L$ and $v_l \sim V_A$, the maximum reconnection rate is $V_{\text{rec}} \sim V_A$. Both features, the simultaneous reconnection events and the broadened reconnection layer, are very important for accelerating particles, as demonstrated in Kowal, de Gouveia Dal Pino, & Lazarian (2011, 2012).

In this work we extend the earlier numerical studies of Kowal, de Gouveia Dal Pino, & Lazarian (2011, 2012) of the acceleration of test particles in collisional, non-relativistic² three-dimensional MHD domains of reconnection having large-scale current sheets with embedded turbulence, in order to assess the dependence of the particles acceleration time and power spectrum with the parameters involved in the process, namely, the reconnection speed which in turn is directly correlated with the Alfvén velocity (V_A), and the turbulence injection power (P_{inj}) and scale ($k_{\text{inj}} = 1/l_{\text{inj}}$) using the same methodology as described in Kowal, de Gouveia Dal Pino, & Lazarian (2012).³

¹ Alternative descriptions of fast reconnection in a collisional MHD scenario have been proposed also by Loureiro, Schekochihin, & Cowley (2007); Shibata & Tanuma (2001).

² Recent studies (Takamoto, Inoue, & Lazarian 2015) indicate that in relativistic domains turbulent driven magnetic reconnection behaves similarly to the non-relativistic case (see Lazarian et al. 2016; de Gouveia Dal Pino, Kowal, & Lazarian 2014, for reviews).

³ We note that in an earlier pioneering work, Kobak & Ostrowski (2000) also studied the role of MHD turbulence in the particle acceleration process in a volume with a reconnecting magnetic field. However, they did not consider a real turbulent cascade developed self-consistently to affect the reconnection at the current sheet, as performed in Kowal, de Gouveia Dal Pino, & Lazarian (2011, 2012) and in the present work. They instead, employed a Monte Carlo method and mimicked the effects of the turbulence with small-amplitude pitch angle scatterings. Their approach did not allow them to detect any Fermi process. Besides, the limitations of their method did not allow them to explore the dependence of the acceleration rate with the parameters of the turbulence, or the Alfvén (and reconnection) velocity, as we do in the present work.

In the next section we summarize the main aspects of the theory of first-order Fermi acceleration within current sheets with fast reconnection driven by turbulence. In Sec. 3, we describe the numerical methodology used in this work to perform the calculations. In Sec. 4.1 we show the computed acceleration time for different models. In Sec. 4.2 we analyse the distribution of the accelerated particles. In Sec. 5 we discuss the results and draw our conclusions.

2 ACCELERATION MODEL

As remarked, in this work we explore the first-order Fermi acceleration process within large-scale current sheets in collisional MHD domains with fast reconnection driven by embedded turbulence. The overall aspects of this mechanism have been thoroughly discussed in several papers and recent reviews (GL05, Kowal, de Gouveia Dal Pino, & Lazarian 2011, 2012; de Gouveia Dal Pino & Kowal 2015) and here we just summarize the main assumptions.

The mechanism of first-order Fermi acceleration operating within large-scale current sheets first proposed by GL05, with trapped particles moving back and forth between the two converging reconnecting magnetic flux tubes, undergoing collisions with magnetic fluctuations and suffering a net energy gain

$$\langle \Delta E/E \rangle \sim V_{\text{rec}}/c \quad (1)$$

after each round trip, is completely general and works either in collisional or collisionless fluids in two and three-dimension domains (Kowal, de Gouveia Dal Pino, & Lazarian 2011). Furthermore, it is equivalent to the first-order particle acceleration process within two-dimensional converging magnetic islands proposed by (Drake et al. 2006), as demonstrated in Kowal, de Gouveia Dal Pino, & Lazarian (2011).

The expression (1) indicates that after several round trips the particle energy must increase exponentially. In addition, it clearly shows that reconnection has to be fast ($V_{\text{rec}} \sim V_A$) in order to make the overall process efficient. For instance, in the surroundings of relativistic sources $V_{\text{rec}} \simeq V_A \simeq c$ (GL05, de Gouveia Dal Pino, Piovezan, & Kadowaki 2010; Giannios 2010; Lazarian 2005)⁴.

Making a simple approximation that particles would escape from the acceleration zone with a similar rate as in shock acceleration, GL05 predicted an analytical power-law energy distribution for the accelerated particles $N(E) \sim E^{-5/2}$ which is actually compatible, e.g., with observed synchrotron power-law spectra slope in microquasars. Relaxing the escape assumption, Drury (2012) found that the particles may leave the acceleration zone with a similar rate as in shock acceleration, which results in $N(E) \sim E^{-1}$ if the compression ratio between the outflow and inflow densities in the reconnection site is large. It is worth noting that the Lazarian & Vishniac (1999) fast reconnection is

built upon an incompressible turbulent theory and the numerical simulations employed here which confirm this (Kowal et al. 2009, 2011, 2012a) were done in the nearly incompressible case, where the inflow/outflow density ratio is close to unity. Indeed, the variations of density in our computational domain are smaller than 5% and are very sensitive to the sonic Mach number. Since our sound speed is 4.0, we have very small sonic Mach number, of the order of 0.25 or smaller. Therefore, Drury's (2012) result does not apply in our context and some anisotropy between the parallel and perpendicular components of the particle velocities is necessary in order to ensure efficient particle acceleration. In Kowal, de Gouveia Dal Pino, & Lazarian (2011, 2012), it has been found that the anisotropy arises from particles preferentially being accelerated either in the parallel or the perpendicular direction in the beginning of the process (see also discussion in de Gouveia Dal Pino, Kowal, & Lazarian 2014; de Gouveia Dal Pino & Kowal 2015). As in Kowal, de Gouveia Dal Pino, & Lazarian (2012), in Section 3 we depict results of numerical simulations of particle acceleration by magnetic reconnection in large current sheets in the presence of turbulence where the evolution of both particle velocity components is tracked separately in order to further address this point.

2.1 Fast reconnection driven by turbulence

In this work we focus on fast reconnection driven by turbulence as described by Lazarian & Vishniac (1999) (see also Eyink, Lazarian, & Vishniac 2011) and tested numerically through three-dimensional simulations by Kowal et al. (2009, 2012). As mentioned in Introduction, in this model, the magnetic field wandering is the key process that induces fast, independent of Ohmic resistivity, magnetic reconnection. The presence of turbulence enables the wandering of the magnetic lines and therefore, reconnection events occurring simultaneously making reconnection very fast. For extremely weak turbulence the reconnection rate reduces to the well known slow Sweet-Parker rate. For further reading on this fast reconnection model we refer to the recent reviews by Lazarian et al. (2012, 2014, 2016).

The predicted dependence of magnetic reconnection on the properties of turbulence, i.e. on the injection power P_{inj} and injection scale of turbulence l_{inj} , is given by (Lazarian & Vishniac 1999; Kowal et al. 2009):

$$\frac{V_{\text{rec}}}{V_A} \propto P_{\text{inj}}^{1/2} l_{\text{inj}}. \quad (2)$$

but the numerical tests by Kowal et al. (2009, 2012) indicate a weaker dependence on l_{inj} , i.e. $V_{\text{rec}}/V_A \propto P_{\text{inj}}^{1/2} l_{\text{inj}}^{3/4}$. In this work we consider the estimated relation between V_{rec} and the turbulence to explore the dependence of the first-order Fermi particle acceleration on the turbulent fast reconnection parameters.

2.2 Particle acceleration within current sheets with fast reconnection driven by turbulence

In a Sweet-Parker reconnection configuration with reconnection made artificially fast by enhanced numerical resistivity, particles are accelerated through a first-order Fermi

⁴ Giannios (2010), in particular, repeated GL05 calculations for a relativistic MHD flow and obtained a net particle energy increase $\langle \Delta E/E \rangle \sim 4\beta_{\text{rec}}/3 + \beta_{\text{rec}}^2/2$, where $\beta_{\text{rec}} = V_{\text{rec}}/c$, which in the limit $\beta_{\text{rec}} \ll 1$ recovers the expression obtained by GL05.

process, as predicted in GL05 and demonstrated numerically in Kowal, de Gouveia Dal Pino, & Lazarian (2011) and Kowal, de Gouveia Dal Pino, & Lazarian (2012). When turbulence is included within the current sheet (see Kowal, de Gouveia Dal Pino, & Lazarian 2012) the acceleration process is improved. As mentioned earlier, this is because the presence of turbulence allows the formation of a thick volume filled with multiple simultaneously reconnecting magnetic lines, making the process intrinsically three-dimensional. Charged particles trapped within this volume suffer several head-on scatterings with the contracting magnetic fluctuations, which significantly improves the acceleration.

The local effective accelerating electric field is $(\mathbf{u} - \mathbf{v}) \times \mathbf{B}$, where \mathbf{u} is the particle velocity, \mathbf{v} is the local velocity of plasma fluctuations, and \mathbf{B} is the local magnetic field (see below).

In the next section we briefly describe the numerical method employed to construct the scenario above and inject test particles, as in Kowal et al. (2012a).

3 NUMERICAL METHODOLOGY

Following Kowal, de Gouveia Dal Pino, & Lazarian (2012), we inject test particles (5,000 - 10,000 protons) into a frozen-in-time 3D MHD domain with a large-scale current sheet containing embedded weakly stochastic turbulence. This domain is built by integrating numerically the collisional MHD equations, which are appropriate for the description of most macroscopic astrophysical flows, until the turbulence in the current sheet reaches a steady-state. Considering that the macroscopic MHD dynamical times are much longer than those of the test particles, using a single snapshot to accelerate the particles is a reasonable assumption (see Sec. 4.1.2).

For each test particle we numerically solve the relativistic equation of motion:

$$\frac{d}{dt}(\gamma m \mathbf{u}) = q(\mathbf{E} + \mathbf{u} \times \mathbf{B}), \quad (3)$$

where m , q , γ and \mathbf{u} are the particle mass, charge, Lorentz factor, and particle velocity, respectively. \mathbf{E} and \mathbf{B} are the electric and magnetic fields, respectively. The electric field is obtained from Ohm's law:

$$\mathbf{E} = -\mathbf{v} \times \mathbf{B} + \eta \mathbf{J}, \quad (4)$$

where \mathbf{v} is the flow velocity, \mathbf{J} is the current density and η is the Ohmic resistivity coefficient. The contribution to the electric field due to the resistivity is neglected, since its effects on the particle acceleration for realistic resistivities are smaller. Therefore, the equation of motion is

$$\frac{d}{dt}(\gamma m \mathbf{u}) = q[(\mathbf{u} - \mathbf{v}) \times \mathbf{B}]. \quad (5)$$

⁵ This equation is integrated in time for the particles using a 4th order Runge-Kutta method, and

⁵ We note that the "collisional" term in our study refers only to the macroscopic MHD flow where magnetic reconnection takes place. The test particles are injected in this flow and then are accelerated due to interactions with local fluctuations through the effective electric field as described by Eq. (5).

Table 1. Turbulent MHD reconnection model parameters, all values are expressed in code units.

Model	I	II	III	IV	V
P_{inj}	1	0.5	0.1	1	1
k_{inj}	8	8	8	12	16

the fields are interpolated up to second order (see Kowal, de Gouveia Dal Pino, & Lazarian 2012).

Particles are initiated with random positions and velocity directions and a thermal velocity distribution. The thermal distribution speed is fixed to $v_{th} = 0.04c$ for all cases. No radiative loss is included, so particles lose or gain energy only by the interactions with the plasma fluctuations.

3.1 Initial Conditions

Distinctly from Kowal, de Gouveia Dal Pino, & Lazarian (2012) who considered only one MHD model of magnetic reconnection, here we explore different conditions for the embedded turbulence in the current sheet. The models studied are described in Table 1.

All models begin with a Harris current sheet $B_x(x, y, z) = B_{0x} \tanh(y/\theta)$, initialized using the magnetic vector potential $A_z(x, y, z) = \ln |\cosh(y/\theta)|$, with a uniform guide field B_{0z} . The initial density profile is set from the condition of uniform total pressure, and the initial velocity is set to zero. The reconnection is initiated by a small perturbation to the magnetic vector potential $\delta A_x(x, y, z) = \delta B_{0x} \cos(2\pi x) \exp[-(y/d)^2]$, with $\delta B_{0x} = 0.05$ and $d = 0.1$ (see also Kowal et al. (2009) for more details).

The velocity and magnetic field are expressed in Alfvén speed units, defined by the antiparallel component of the magnetic field, and the initial unperturbed density $\rho_0 = 1$. The initial strength of the antiparallel component of the magnetic field is set to $B_{0x} = 1.0$ in all models, and the guide field to $B_{0z} = 0.1$. The distance unit is defined by the length of the computational box in the x direction. The box has size $L_x = L_z = 1$ and $L_y = 2$. The time is measured in units of L_x/V_A . The computational box has a grid of $256 \times 512 \times 256$ for all models. For more details see Kowal et al. (2009) and Kowal et al. (2012).

Turbulence is driven using a method described in Alvelius (1999). The driving is made by injecting discrete velocity fluctuations in the Fourier space concentrated around the wave vector k_{inj} , corresponding to the injection scale l_{inj} . The amplitude of driving is solely determined by its power P_{inj} , the number of driven Fourier components, and the time step of driving. In all models the turbulence is sub-Alfvénic. See Kowal et al. (2009) for further details. When the turbulence is developed and reach a steady-state, we injected test particles in this domain and followed their trajectories according to Eq. (5). The turbulence injection power and length scale for the studied models are given in Table 1.

A map illustrating the trajectory of an injected test particle in the 3D magnetic reconnection domain is depicted in Figure 1.

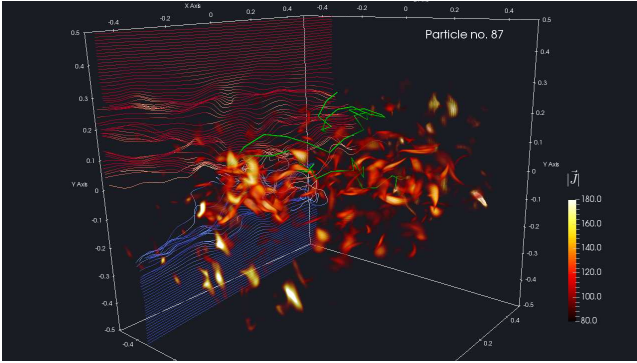


Figure 1. This map illustrates the trajectory (in green) of an injected test particle bouncing up and down in the 3D magnetic reconnection domain simulated with turbulence embedded in it to drive fast reconnection. The volume depicts the current sheet region with several very high current density patches where the test particle is scattered by magnetic fluctuations while accelerated. The blue and red lines represent the two magnetic line fluxes of opposite polarity.

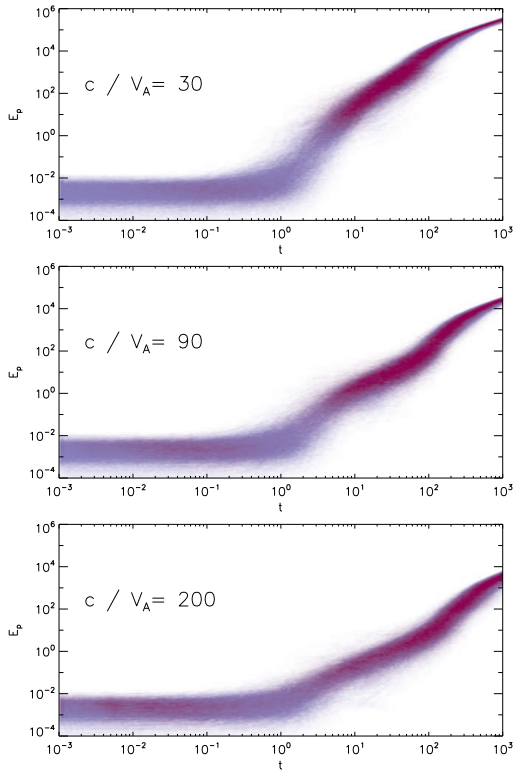


Figure 2. Proton kinetic energy evolution for $c = 30, 90$ and $200 V_A$ for model I. The colors correspond to particles accelerating their parallel (red) and perpendicular (blue) components of velocity with respect to the local mean field.

4 RESULTS

4.1 Acceleration time

As mentioned above and from Eq. (2), the reconnection rate V_{rec} in the presence of turbulence, for a fixed value of the anti-parallel magnetic field component ($\equiv V_A$), depends only on P_{inj} and its injection scale k_{inj} (l_{inj}). The

acceleration rate is naturally expected to depend on V_{rec} (de Gouveia Dal Pino & Kowal 2015). In what follows we study the dependence of the acceleration time on V_A/c , P_{inj} and l_{inj} .

For computing the mean acceleration time as a function of energy, we calculate $t_{\text{acc}} = \sum_{i=1}^{N_E} t_i / N_E$ where N_E is the number of particles with energy between E and $E + \Delta E$, and t_i is the acceleration time of particle i ; the corresponding standard deviation is $\sigma^2 = \sum_1^{N_E} (t_{\text{acc}} - \bar{t})^2 / (N_E - 1)$.

4.1.1 Dependence of the acceleration time on V_A/c and the particle energy

For fixed different values of the turbulence injection parameters we study the particle acceleration as a function of V_A/c .

In Figure 2 we show the kinetic energy evolution in logarithmic diagrams for $c = 30, 90$ and $200 V_A$ for model I. The initial particles distribution is the same in all cases. Particles are injected with a thermal distribution with a temperature corresponding to the sound speed of the isothermal MHD model (see Kowal, de Gouveia Dal Pino, & Lazarian 2011). The maps depict energies for both the parallel (red) and the perpendicular (blue) particle velocity components⁶. Initially, particles suffer drift acceleration under the effect of the magnetic field gradients, which is slow (see the left part of each diagram up to $t = 10^0$); when they arrive in the current sheet they start bouncing back and forth between the converging magnetic fluxes: the first order Fermi process starts operating (see Figure 5 in Kowal, de Gouveia Dal Pino, & Lazarian 2011). The diagrams in Figure 2 clearly indicate that the particles energy increases very fast up to a maximum value.⁷ After reaching this maximum energy, the particles are no longer confined to the current sheet and the stochastic mechanism saturates. This can be inferred in the energy evolution, which exhibits a change in the growth rate at around $t = 2 \times 10^2$. After that, particles continue to accelerate, at a slower rate, possibly due to the drift acceleration (see also Kowal, de Gouveia Dal Pino, & Lazarian 2012). As we decrease V_A , the acceleration process takes slightly longer time to start, as depicted in Figure 2. The maximum energies that particles reach also change with V_A , as it can be clearly seen in Figure 2. The maximum energies for $c = 30, 90$ and $200 V_A$ are approximately around $10^4 m_p c^2$, $6 \times 10^3 m_p c^2$ and $10^3 m_p c^2$, respectively.

In the absence of losses, the maximum energy that particles can reach (accelerated by the first order mechanism) depends on the size of the acceleration region (the effective

⁶ The number of particles being accelerated preferentially in the perpendicular or parallel direction is counted considering: $u_{\parallel} > u_{\perp}$ and $du_{\parallel}/dt > 0$ in the parallel case, and $u_{\perp} > u_{\parallel}$ and $du_{\perp}/dt > 0$ in the perpendicular one.

⁷ We note that the regime of faster increase in the log-log diagrams of Figure 2, actually reflects the exponential growth of the energy with time for each of the thousands of accelerated particles (Figs. 4 and 5 of Kowal, de Gouveia Dal Pino, & Lazarian 2011 show this exponential growth of energy for each test particle more clearly). This increase, which in the log-log diagrams is provided by the collective behaviour of all particle sample - can be fitted by power laws with indices > 2 (see Kowal, de Gouveia Dal Pino, & Lazarian 2012).

thickness of the reconnection layer) and on the value of the magnetic field. Indeed, in order to be confined the particle Larmor radius should be smaller than the thickness of the acceleration region l_{acc} ⁸. The maximum energy is then

$$E_{\text{max}} \simeq e l_{\text{acc}} B, \quad (6)$$

hence it changes with B (or V_A/c).

If we take the thickness of the acceleration region l_{acc} as the width of the current sheet predicted from mass conservation, $\Delta \simeq L(V_{\text{rec}}/V_A)$, where L is the length of the reconnection layer which in our case is the size of the computational domain, then according to Lazarian-Vishniac theory $E_{\text{max}} \simeq \sqrt{4\pi\rho} P_{\text{inj}}^{1/2} l_{\text{inj}} V_A^{-1/2}$ (e.g., [Eyink, Lazarian, & Vishniac 2011](#)). However, in the 3D simulations employed here (see also, [Kowal, de Gouveia Dal Pino, & Lazarian 2012](#)) the turbulence was injected in a region around the current sheet of thickness $\sim 0.4L$, therefore, the maximum energy should be constrained by $0.4L$ rather than by Δ and in this case $E_{\text{max}} \propto 0.4L B \propto 0.4L V_A$. This is consistent with the values of the maximum energies inferred from Figure 1 which increase with V_A .

Figure 3 shows the parallel and perpendicular mean acceleration times, as functions of the kinetic energy for $c = 20 - 1000 V_A$, for the same MHD fast reconnection model (model I). The evolution of both particle velocity components, parallel and perpendicular to the magnetic field, is tracked separately, in order to detect anisotropies that may be important for particle confinement, as mentioned above. The energy is in $m_p c^2$ units.

The acceleration time in Figure 2 can be fitted by a power law in energy, $t_{\text{acc}} \propto E_p^\alpha$, where α can be estimated for a given energy band as $\alpha = \Delta \log(t_{\text{acc}}) / \Delta \log(E_p)$.

Figure 3 presents index α as a function of the kinetic energy for the parallel and perpendicular acceleration for different values of c/V_A of model I. In both cases, there is a peak in α around $1.5 - 2.0$ at very low energies ($\sim 10^{-2}$). From Figure 2, we see that this peak occurs when particles are undergoing the initial slow drift acceleration (due to the spatially varying magnetic field) just before they enter the reconnection region (see also Figure 5 in [Kowal, de Gouveia Dal Pino, & Lazarian 2011](#)). When particles enter the fast (exponential) acceleration regime in the reconnection zone (Figure 2), α drops quickly to values below ~ 0.6 (at energies $\sim 10^{-1}$), therefore increasing the acceleration rate. In this regime, α remains within the range from 0.2 to 0.6, until the energy reaches the saturation value and α starts to increase again very smoothly as particles undergo further drift acceleration, outside the reconnection region, in agreement with Figure 2.

Figure 5 shows the averaged value of α as a function of V_A/c for the parallel and perpendicular components for model I. In these diagrams, in order to evaluate α only in the regime of faster (first-order Fermi) acceleration, we have selected the energy ranges for averaging α starting at $E_p \sim 3 \cdot 10^{-2}$ up to 10^0 , 10^1 , 10^2 , and 10^3 . The values of α span from 0.2 to 0.6. For $20 < c/V_A < 1000$ the indices

⁸ We are not considering radiative losses, but for protons they may be important under extreme conditions.

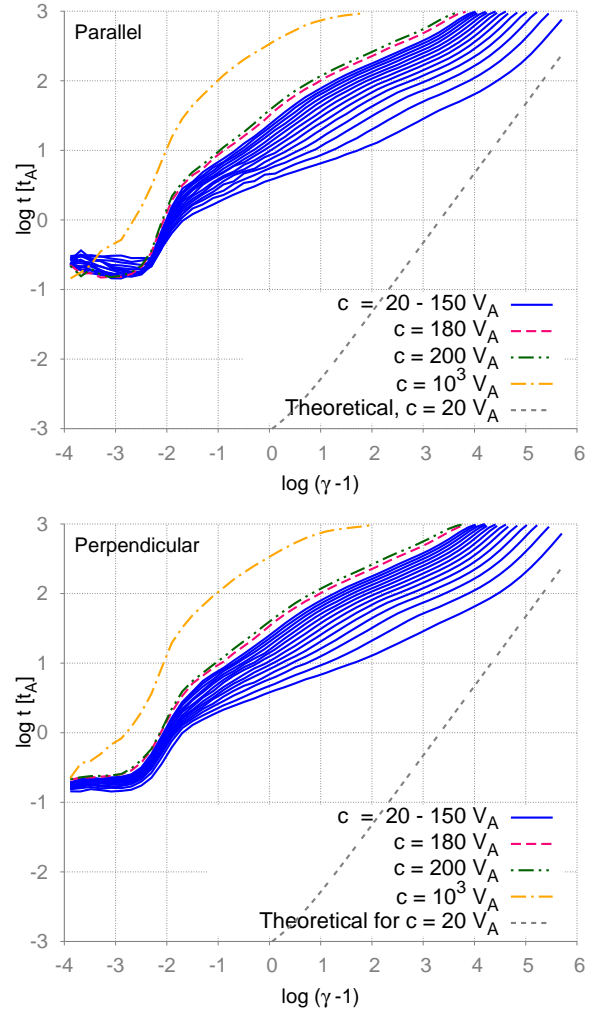


Figure 3. Acceleration time as a function of particle kinetic energy (normalized by the rest mass) for different values of c/V_A , from 20 to 1000, for both parallel (upper panel) and perpendicular particle velocity components (bottom panel) for model I. The blue lines correspond to values c/V_A from 20 to 150, with $\Delta(c/V_A) = 10$. The dashed grey line gives the predicted minimum acceleration time (Eq. 7) t_{thr} for the model with $V_A = c/20$.

are almost independent of the averaging energy band, as in Figure 4. For $c/V_A < 20$, the turbulence inside the reconnection region is in the relativistic regime and the MHD simulations considered in this work are expected to be no longer valid. This explains the increase of α seen in Figure 5 for the smallest values of c/V_A and thus a decrease of the acceleration rate where we expected the opposite. For c/V_A around 60 and above, the index starts to strongly depend on the averaging energy band making the error bars much larger, and suggesting a trend of saturation of the value of α in this low V_A (and reconnection velocity) region. We further notice that the blue lines in these diagrams, which give the value of α averaged in the low energy band (between 0.03 and 1) is dominated by the region in Figure 2 right before the entering into the zone of fast acceleration. Since the differences of the α values estimated for different energy bands are still smaller than error bars, we can conclude that the characteristic values of α in the first-order Fermi regime

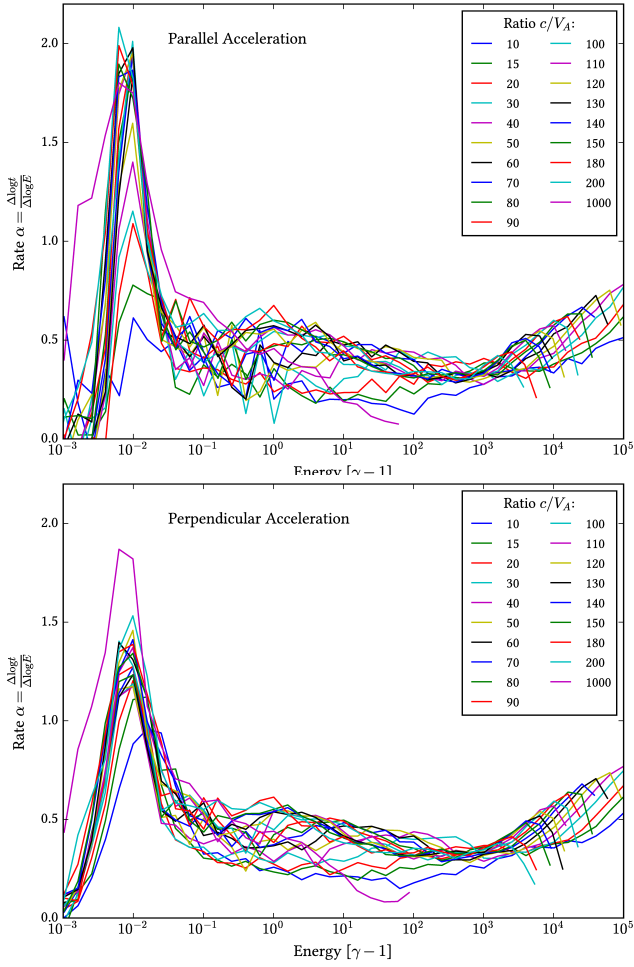


Figure 4. Power-law index α of the acceleration time for both parallel (up) and perpendicular acceleration (bottom) as a function of the kinetic energy.

lie between $0.2 < \alpha < 0.6$ for a large range of values of c/V_A , both for the parallel and perpendicular acceleration components.

Now, going back to Figure 3, we can estimate analytically the minimum acceleration time as (e.g., de Gouveia Dal Pino & Kowal 2015):

$$t_{\text{thr}} = \frac{E}{eBV_{\text{rec}}}. \quad (7)$$

In Figure 3 we show the value of t_{thr} calculated for $V_A = c/20$, and $V_{\text{rec}} \sim 0.1 V_A$. We clearly see that the acceleration times we obtained for the model with $V_A = c/20$ are longer than this lower limit t_{thr} which is attained only for the maximum energy in the upper right part of the diagram, as one expect since the expression above is actually valid for the maximum energy (see Eq. 6).

The above results are compatible with the notion that the acceleration time t_{acc} must decrease with V_{rec}/c (see also Eq. 1). To explore more quantitatively this issue, we show in Figure 6 the acceleration time as a function of V_A/c for different proton energies $E = m_p c^2$, $10 m_p c^2$ and $10^2 m_p c^2$. For computing t_{acc} in physical units we consider Alfvén time $t_A = L/V_A$, with $L = 1$, the same time units as in the MHD simulations. The acceleration time t_{acc} decreases with V_A/c for a fixed energy E . Figure 6 also shows the best fitted

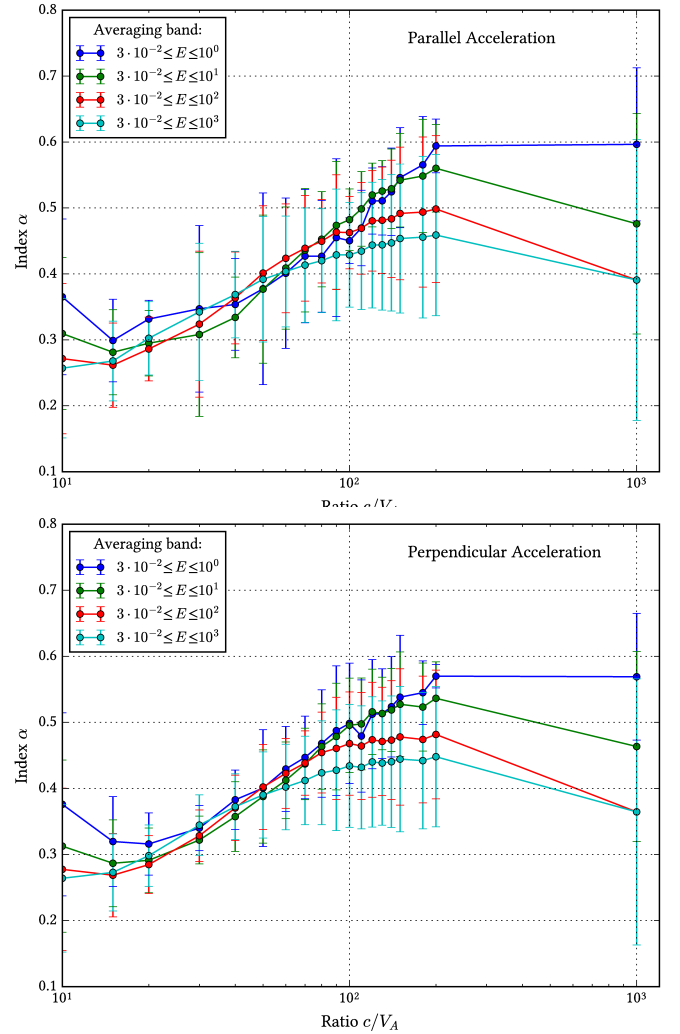


Figure 5. Power-law index α of the acceleration time for both parallel (up) and perpendicular acceleration (bottom) as a function of the V_A/c ratio.

function $t_{\text{acc}}(V_A/c)$. For the three example energies considered here we get $t_{\text{acc}} \propto (V_A/c)^{-\kappa}$, with $\kappa = -2.09 \pm 0.06$, -2.34 ± 0.03 and -2.35 ± 0.03 , respectively. The acceleration time in a DSA process scales with $(V_s/c)^{-2}$, where V_s is the shock velocity; in the acceleration by reconnection it seems that there is a stronger dependence on V_A/c , at least at high energies.

4.1.2 Dependence of the acceleration time on the environment evolution

We have also computed the acceleration time of the particles injected in three different dynamical time steps of the MHD turbulent reconnection site for model I, after the turbulence reached a statistical steady state. The time scale of the MHD environment is assumed to be much longer than the particles time scales, therefore we expect no significant changes in the particles evolution and acceleration when considering different dynamical times of the same MHD reconnection model (Kowal, de Gouveia Dal Pino, & Lazarian 2012). From the

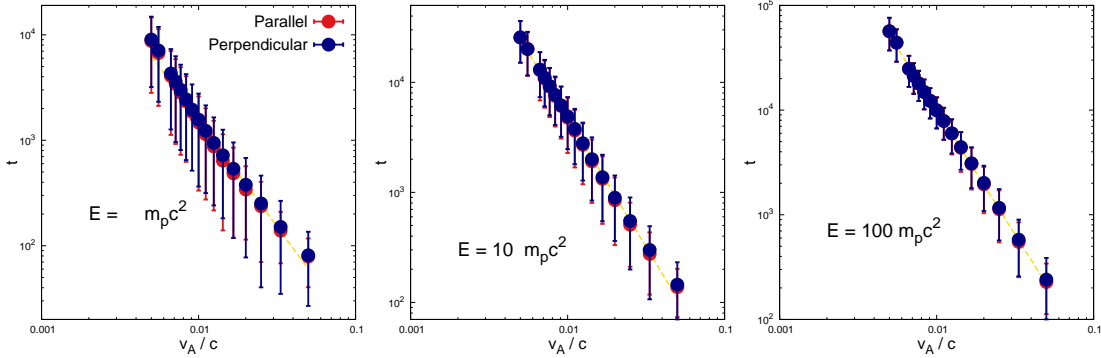


Figure 6. Mean acceleration time as a function of V_A/c , for both parallel and perpendicular particle velocity components, for different proton energies $E = m_p c^2$, $10 m_p c^2$ and $10^2 m_p c^2$. The yellow line is the best-fitted function $t_A \propto (V_A/c)^{-\kappa}$ (see text).

computed acceleration times for the three simulated time steps of Model I, for both parallel and perpendicular components, we conclude that there is no significant change as expected. We have found the same behaviour for all values of c/V_A (as seen in Figure 3). Also, a similar power law $t_{\text{acc}} \propto E_p^\alpha$ with an index $\alpha \sim 0.4$ at relativistic energies is observed for these three dynamical times.

4.1.3 Dependence of the acceleration time on P_{inj}

The reconnection rate increases with the injection power (see Eq. 2) and therefore, the acceleration rate is also expected to increase for larger P_{inj} . We computed the mean acceleration time for models II and III and compared them with model I, in order to test the dependence of the acceleration efficiency on the turbulent power. Figure 7 shows mean acceleration times as functions of E for $c = 50 V_A$, for both velocity components. We clearly see that for energies smaller than the saturation value, i.e., in the region of fast acceleration, the acceleration efficiency increases with P_{inj} (corresponding to shorter acceleration time t_{acc} , as expected from Eq. (1)), although the differences within an order of magnitude are, in general, encompassed by the error bars. For models II and III the power-law index in the relation $t_{\text{acc}} \propto E^\alpha$ is a little steeper, with $\alpha > 0.4$. At energies larger than the saturation value (around $\gamma - 1 = 10^3$ for models II and III and $\gamma - 1 > 10^5$ for model I), the maximum acceleration times are similar in all models.

The weak dependence seen of the acceleration time with P_{inj} can be attributed to the fact that particles are accelerated while being scattered by the turbulent magnetic fluctuations in the plasma ($\mathbf{v} \times \mathbf{B}$). For larger injection power the velocity (and magnetic) fluctuations are stronger and therefore, the time the particles remain confined in turbulent patches gaining energy may be longer than in a case with smaller injection power.

4.1.4 Dependence of the acceleration time on k_{inj}

According to Eq. (2), the reconnection rate V_{rec} is also expected to increase with injection scale of the turbulence $l_{\text{inj}} \sim 1/k_{\text{inj}}$. We computed the mean acceleration time for models IV and V and compared with model I to test this dependence. Figure 8 shows the mean acceleration time as

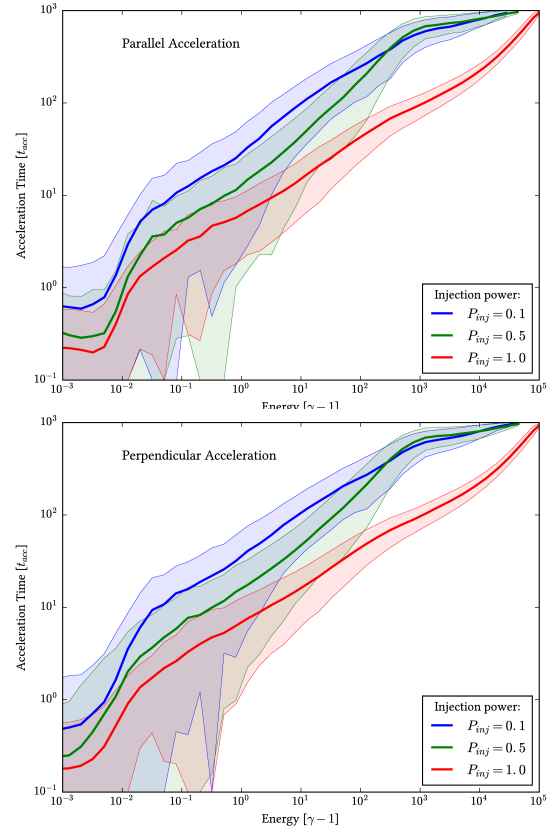


Figure 7. Mean acceleration time as a function of E for both parallel (top) and perpendicular (bottom) acceleration for models I, II and III with different turbulence injection power P_{inj} and the same injection scale $k_{\text{inj}} = 8$ (see Table 1). All models have $c = 50 V_A$.

a function of E for $c = 50 V_A$, for both, parallel and perpendicular, acceleration components with transparent areas corresponding to the estimation error of t_{acc} . For energies smaller than 10^1 , there is no dependence on the injection scale, which could be attributed to the fixed size of the turbulent region in all models. However, for larger energies we observed the expected behaviour, where the efficiency of acceleration increases, or the acceleration time t_{acc} decreases with the decrease of k_{inj} . Although the differences are again

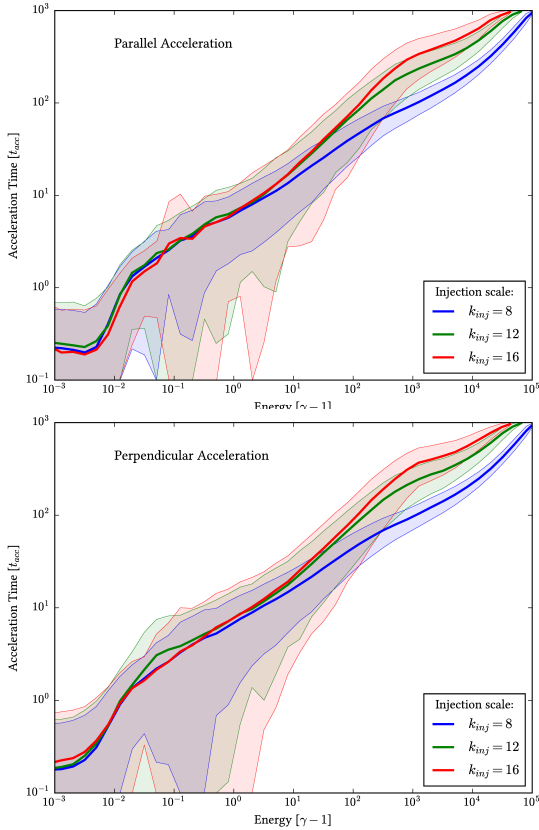


Figure 8. Mean acceleration time as a function of E for both parallel (top) and perpendicular (bottom) acceleration for models I, IV and V with different turbulence injection scales k_{inj} and the same injection power $P_{inj} = 1$ (see Table 1). All models have $c = 50V_A$.

within an order of magnitude at most (before the saturated energies are reached) and generally encompassed by the error bars. For models IV and V, the slopes of the relation $t_{acc} \propto E^\alpha$ in the region of fast growth are also slightly steeper than in model I, with $\alpha > 0.4$.

Comparing Figures 7 and 8, we note that the acceleration time for a given E has a slightly stronger dependence on P_{inj} than on k_{inj} , particularly at the highest energies near the saturation of the fast growth. According to Eq. (2) one might expect the opposite, i.e., a stronger dependence on k_{inj} . Nevertheless, we have also remarked already that the numerical simulations of Kowal et al. (2009) predict a weaker dependence of V_{rec}/V_A on k_{inj} than that predicted in Eq. (2) and thus we might expect that this would reflect in the results for the acceleration time as well.

4.2 Distribution of the accelerated particles

The protons initially have a thermal distribution, with the same thermal speed for all models. The particles begin to gain energy slowly until the Fermi mechanism starts operating. In Figure 9 the distribution of particles at $t = 0.07 t_A$ after the injection is shown for the parallel and perpendicular components of velocity; the color lines represent different values of c/V_A (from 20 to 200); only accelerated particles are plotted. The initial distribution is the same for all values of V_A/c . The number of particles accelerated in the direction

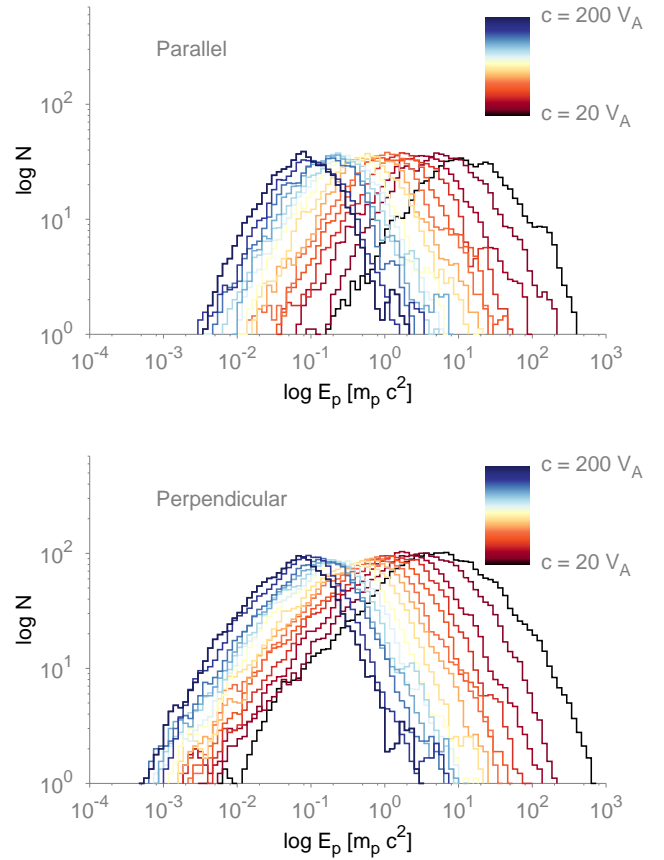


Figure 9. Distribution of the number of particles as a function of the particle energy in units of $m_p c^2$ for different values of c/V_A from 20 to 200, for both the parallel (left panel) and the perpendicular (right panel) components. t is $0.07 t_A$ after the injection, for all c/V_A models (the other parameters correspond to those of Model I class in Table 1).

perpendicular to the local magnetic field is larger than that of the particles accelerated in the parallel direction. For the largest V_A higher energies have already been reached and the distributions are wider in energy. In the most efficient acceleration case (the highest V_A/c) the distribution already exhibits a power-law tail due to the Fermi acceleration (see Kowal, de Gouveia Dal Pino, & Lazarian 2011, 2012).

In Figure 10 the evolution of the proton distribution during the acceleration is shown, for the parallel (red lines) and perpendicular velocity components (blue lines) to the local magnetic field. The seven time steps exhibited in the figure correspond to $t = 10^{-0.6}, 10^0, 10^{0.49}, 10^{0.89}, 10^{1.97}, 10^{2.5}, 10^3 t_A$. We show the distributions for the $c = 30, 90$ and $200 V_A$ cases of model I. The evolution of the particle distribution is similar for all values of c/V_A . Initially, the particles have a normal distribution (not shown here) and, as particles gain energy, they start to populate higher values of energy. At some point (see the second curve from left to right in each diagram) the distribution becomes flatter than a normal distribution at higher energies. Due to our numerical setup, particles never stop accelerating as they are continuously reinjected into the system and therefore, the distribution shifts to higher and

higher energies. As remarked, even after the particles attain the maximum energies allowed in the reconnection region by the first-order Fermi process, they suffer further drift acceleration at a smaller rate. Thus, in the absence of radiative losses or a escape from the acceleration region, the particles may gain energy continuously. Most of the particles reach very high energies as time evolves. Their distribution may even get a positive power-law index in very evolved times (as we can see in the figure), but of course in real systems we should expect an interruption of this acceleration process with the escape of the particles from the finite volume of the acceleration zone and/or due to radiative losses.

It is interesting to note that for all V_A/c cases shown in Figure 10 there are more particles being accelerated in the perpendicular than in the parallel direction to the local magnetic field. This anisotropy ensures the success of the acceleration process (see discussion in de Gouveia Dal Pino & Kowal 2015, and references there in). The effective electric field accelerating a particle (with velocity \mathbf{u}) is given by Eq. (5) and may lead to both parallel and normal acceleration directions to the local mean field depending on the original direction of the interacting magnetic fluctuation of the turbulent flow (\mathbf{v}), or in other words on the resulting direction of $(\mathbf{u}-\mathbf{v})$ with respect to the local \mathbf{B} (given by the sum of the mean plus the fluctuating component). Nevertheless, the fact that we see in Figure 10 more particles in the perpendicular direction than in the parallel direction is an indication that the effective electric field is predominant in the normal directions on average.

During the total integrated time considered in Figure 10, $t_f = 10^3 t_A$, the particles in models with larger V_A/c reach higher energies. Since the size of the system L is independent of V_A and is the same for all models, naturally models with larger ratios c/V_A and thus larger acceleration rate will accelerate particles to higher energies (at the same time interval). We should point out that in the cases shown in this Figure, the maximum energy achievable by the first-order mechanism (at the saturation of the fast growth) has already been reached at $t = t_f$ (see Figure 2).

As stressed above, since in our simulations the particles are continuously accelerated and there is no physical mechanism to allow them to escape, it is not possible to obtain the actual distribution of the accelerated particles. Nonetheless, we can make some estimate of the power-law index of the distribution soon after the particles start to populate the high-energy tail.

In Figure 11 we show the total number (not only the accelerated ones) of particles as a function of energy for two different time steps. Each figure corresponds to the cases $c/V_A = 30, 90$ and 200 of Model I. The initial normal distribution ($t = 0$) is shown in gray dashed lines. The earliest time step plotted in each case corresponds to the approximate time when a high-energy power-law tail starts to form (i.e., when particles reach kinetic energies larger than $\sim 10^{-2} mc^2$, according to Figure 2); the second time corresponds to a little longer time step. In each time step we can distinguish two components in the distributions: a normal one (shown in solid gray line) + a power-law tail that fits the high energies starting at a certain energy we denote as E_{pl} . We see that the first power-law index at the earlier times can be fitted by $\sim p = -1.3$ to -1 . However, these values would be a little smaller (corresponding to slightly steeper spectra)

if we had taken the spectra at a little earlier time. Therefore, these values can be taken as approximate ones. The second power-law at later times in all the cases is flatter due to the effects discussed above and therefore, they must be taken only as illustrative of the limitations of the method. Of course, in realistic systems, the presence of physical particle escape from the acceleration zone, radiative losses and dynamical feedback of the accelerated particles into the plasma will result in steeper spectrum in the late times too ($|p| > 1$). We have also estimated the percentage of particles with energies $E > E_{pl}$ (populating the high-energy region of the distribution). In all the cases this percentage increases from the first to the second time step.

4.2.1 Dependence of the particles spectrum on P_{inj}

For all models of Table 1, the particle distribution behaves in the same way as in model I above; as particles reach higher energies they start to develop a power-law. The anisotropic distributions with the production of more accelerated particles in the perpendicular than in the parallel direction are also present in models II and III (for the studied cases $c/V_A = 50, 100$, and 150).

A considerable dependence on P_{inj} is found in the evolution of the distribution of the accelerated particles. At each given time, model I which has the largest injection turbulence power, more particles accelerate and reach higher energies than in other models of Table 1. The differences increase with energy, in consistency with Figure 7. Model III is the less efficient as expected. Models I and II reach relativistic energies and exhibit a high-energy power-law tail at $t = 10^0 t_A$, while model III only shows this behaviour at a later time.

4.2.2 Dependence of the particles spectrum on k_{inj}

We also compared the particles energy distribution of Models IV and V with Model I, differing only in the turbulence injection wavenumber k_{inj} (according to Table 1), for the cases $c/V_A = 50, 100$ and 150 . As in Model I, the other models also exhibit similar anisotropy with more particles being accelerated in the perpendicular than in the parallel direction to the local magnetic field. We also found a weaker dependence in the evolved spectrum with k_{inj} than with P_{inj} , as before (see Figures 7 and 8). The differences between the distributions become more relevant at the high energies near the saturation of the fast growth region, with the distribution in Model I slightly flatter than in Models IV and V, respectively, but within the error bars the distributions are very similar.

4.2.3 Effects of the initial particle energy distribution

In all the models studied so far, we considered the same initial thermal particle distribution with a thermal speed $v_{th} = 4c/100$. This distribution corresponds to an initial energy $E \sim 5 \times 10^{-4} m_p c^2$. We have also computed the acceleration of particles for a model with the same turbulence properties of model I and with $V_A/c = 50$, but changing the initial particle distribution, considering two other cases: one with a larger thermal speed ($v_{th} = 4c/10$) and the other

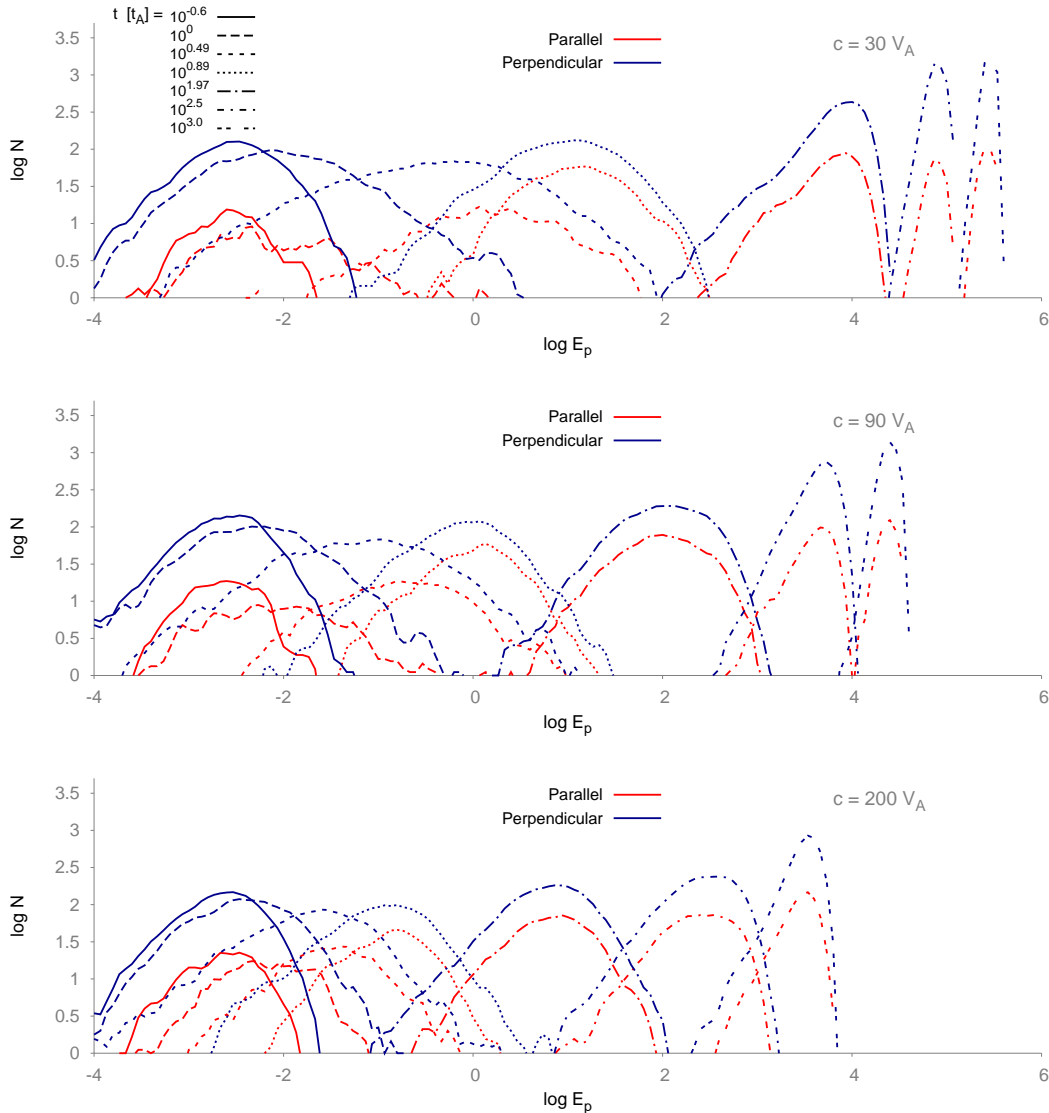


Figure 10. Evolution of the number of accelerated particles (both for the parallel (red lines) and perpendicular (blue lines) velocity components) for $t = 10^{-3}t_A$ to $t = 10^3t_A$. We show the cases $c/V_A = 30$ (top), 90 (middle) and 200 (bottom) for model I of Table 1. The energy is in units of $m_p c^2$. The seven time steps exhibited from left to right correspond to $t = 10^{-0.6}, 10^0, 10^{0.49}, 10^{0.89}, 10^{1.97}, 10^{2.5}$ and $10^3 t_A$.

with a smaller one ($v_{th} = 4c/1000$) than Model I. When comparing the acceleration rates of these three cases we find that after some time they all behave identically, i.e., the initially less energetic particle distribution takes longer time to enter the magnetic reconnection acceleration zone, but once the particles start to be accelerated, they evolve similarly to the other distributions, particularly after reaching values of the Lorentz factor $\gamma > 1$.

Figure 12 depicts the particles distribution after a time, $t = 0.5 t_A$ for the three cases. The best fitted total (normal + power-law) distribution is also shown for each model. We see that they all produce a similar power-law, independently of the initial thermal energy of particles.

5 SUMMARY AND DISCUSSION

In this work we have investigated the first-order Fermi acceleration of particles within large-scale current sheets with fast magnetic reconnection driven by turbulence, using 3D collisional MHD simulations with the injection of test thermal particles, following the same approach as in (Kowal, de Gouveia Dal Pino, & Lazarian 2012). We extended here this earlier study (see also Kowal, de Gouveia Dal Pino, & Lazarian 2011; de Gouveia Dal Pino, Kowal, & Lazarian 2014; de Gouveia Dal Pino & Kowal 2015) by examining the effects of the parameters of the reconnection on the effective acceleration rate and the evolution of the spectrum of the particles. We considered models with different values of V_A/c and different turbulence injection scale and power.

The main results can be summarized as follows.

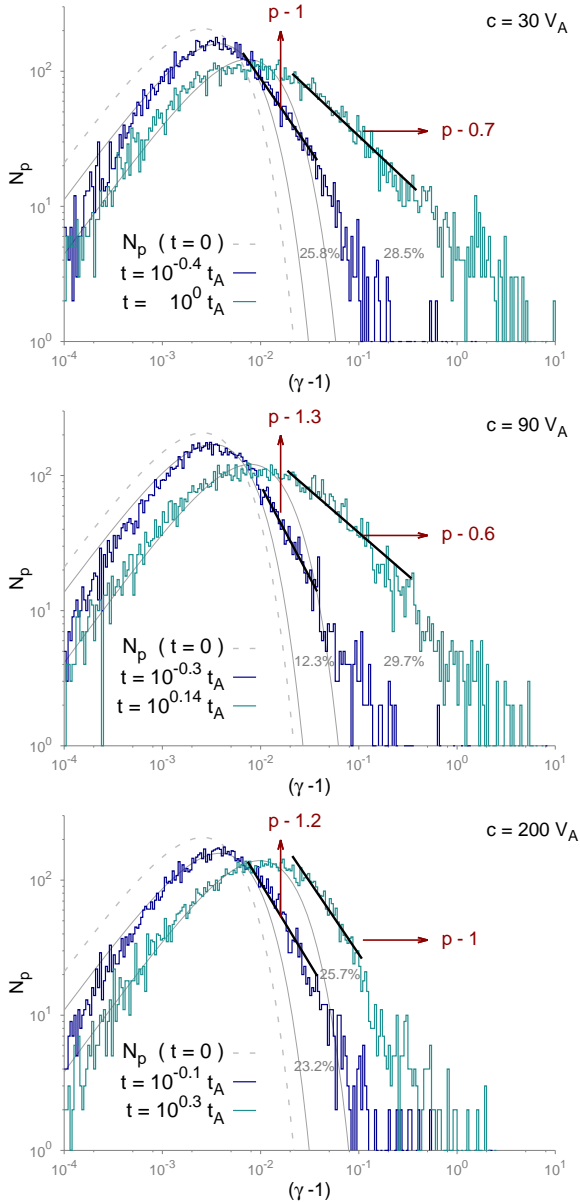


Figure 11. Total particle distribution as a function of the normalized energy at two different timesteps for (from top to bottom) the $c/V_A = 30, 90$ and 200 cases of Model I. The dotted gray line is the initial normal distribution, which is the same for all cases. Each distribution can be fitted by a normal distribution (shown in solid gray line) plus a power-law distribution.

- The acceleration time follows a power-law dependence with the particle energy, $t_{acc} \propto E^\alpha$, with $0.2 < \alpha < 0.6$ which is weakly sensitive to the magnetic reconnection parameters of the injected turbulence, tested for a large range of values of $c/V_A \sim 20 - 1000$.

- The acceleration time dependence with the Alfvén velocity is $t_{acc} \propto (V_A/c)^{-\kappa}$, with $\kappa \sim 2.1 - 2.4$ for particle kinetic energies between $E = (1 - 10^2) m_p c^2$, respectively and keeping the same trend approximately for larger energies (tested for model I).

- For a given value of the V_A/c ratio, the acceleration time is shorter for larger values of the turbulence injection param-

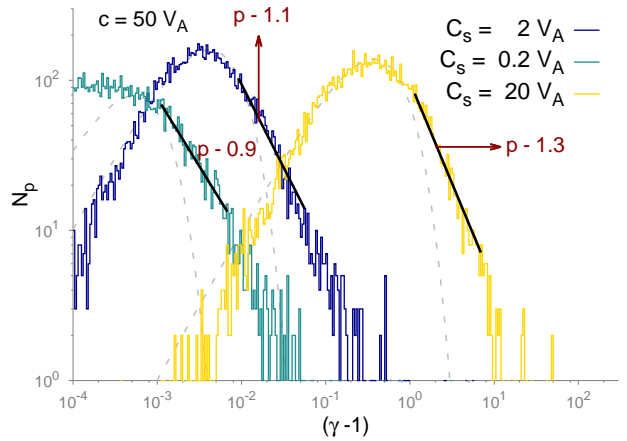


Figure 12. Histograms of the number of particles for three different initial particle distributions for model I with $C_s = 4c/10, 4c/100$ and $4c/1000$. In all the cases $c/V_A = 50$ and $t = 10^{-0.3} t_A$.

eters, i.e. l_{inj} and P_{inj} , as expected from theory. Nonetheless, the maximum differences between the models are generally less than an order of magnitude and are within the error bars due to the uncertainties in the evaluation of the acceleration times from the numerical simulations, so that we can conclude that these dependences are not relevant.

- In all the cases studied here, the number of particles being accelerated in the perpendicular direction to the local magnetic field is larger than the ones being accelerated in the parallel direction. This unbalancing is important to ensure the effectiveness of the acceleration process (see below).

- The particle spectrum of the accelerated particles develops a high-energy tail, which can be fitted by a hard power-law index $\propto E^p$, with $p \sim -1.3$ to -1 (or even a little smaller) in the early times of the acceleration and is independent of the initial thermal energy of the injected particle distribution.

These results have important implications for studies of particle acceleration specially in magnetically dominated regions of astrophysical environments like the surroundings of GRBs, black holes in AGNs and microquasars, and the relativistic jets associated to these sources. As remarked, most studies of first-order Fermi particle acceleration by magnetic reconnection have been performed considering PIC simulations (e.g., Zenitani & Hoshino 2007; Lyubarsky & Liverts 2008; Drake et al. 2010; Cerutti et al. 2013; Sironi & Spitkovsky 2014; Guo et al. 2014, 2015), which apply only to the kinetic scales of the flow. In order to probe the large-scale properties of the acceleration by magnetic reconnection beyond the kinetic scales in collisional astrophysical systems like those mentioned above, an MHD description is required. The 2D and 3D studies undertaken by Kowal, de Gouveia Dal Pino, & Lazarian (2011, 2012) and in this work have explored exactly these macroscopic scales of the acceleration by magnetic reconnection and thus are complementary to the former kinetic studies.

It should be noticed also that, contrary to what has been found in PIC simulations (e.g., Guo et al. 2014), Kowal, de Gouveia Dal Pino, & Lazarian (2011) demonstrated that the acceleration of energetic particles in 2D and 3D reconnection domains shows substantial differences, be-

ing more efficient in the second case. This justifies why our analysis here has focussed on 3D geometries of reconnection only.

The earlier collisional numerical studies (Kowal, de Gouveia Dal Pino, & Lazarian 2011, 2012; see also Dmitruk & Matthaeus 2003) and most of the ones presented here have neglected the time evolution of the MHD environment. This is in general expected to be valid since this time is much longer than the particle time scales, particularly when considering a first-order Fermi process in a statistically steady state turbulent domain. In Sec. 4.1.2, we explored the particle acceleration considering different snapshots of the reconnection domain and found no significant changes, as predicted. Nonetheless, this evolution may be important when considering more realistic non-steady flows and when calculating the spectra and loss effects in real astrophysical systems. Preliminary steps in this direction have been performed in studies like, e.g. Lehe, Parrish, & Quataert (2009); Khiali, de Gouveia Dal Pino, & del Valle (2015); Khiali & de Gouveia Dal Pino (2016); Khiali, de Gouveia Dal Pino, & Sol (2015).

Earlier analytical studies of the first-order Fermi process in large-scale current sheets (e.g., GL05; Drury 2012) predicted that the acceleration time would be similar to that of shock acceleration, and the energy power-law spectrum of the accelerated particles could be either steeper or harder than the one predicted for shock acceleration and nearly independent on the reconnection velocity. These predictions, although based on rather simplified assumptions have been at least qualitatively confirmed by the results of this work. For a broad range of reconnection velocities represented by a fiducial parametric space encompassing $V_A/c \sim 1/1000 - 1/20$, the acceleration time dependence with the kinetic particle energy is found to be $\propto E^\alpha$, with $\alpha \simeq 0.2 - 0.6$.

Furthermore, the minimum analytically estimated acceleration time according to Eq. (7) is comparable to the values found in the simulations when the particles reach the maximum energy during the first-order Fermi acceleration in the reconnection zone (the saturation energy). As we have seen, this maximum energy is attained when the particle Larmor radius becomes comparable to the size of the acceleration zone.

It is also remarkable that the power-law indices obtained for the particles distribution in the high-energy tail from our collisional MHD simulations in the large scales are comparable to the values obtained from the PIC simulations in the kinetic scales of the plasma (e.g., Zenitani & Hoshino 2001; Drake, Swisdak, & Fermo 2013; Sironi & Spitkovsky 2014; Guo et al. 2014, 2015; Li et al. 2015).⁹

We should stress that the acceleration process in magnetic reconnection sites with turbulence theory depends on

V_A , P_{inj} and l_{inj}) that determines the first-order energy gain; (ii) the thickness of the turbulent region which improves the particle scattering probability; and (iii) the strength and maximum scale of the velocity and magnetic field fluctuations within the turbulent region, which control the scattering mean free path (or time) which in turn depend on both P_{inj} and l_{inj} . Therefore, the overall acceleration process is very complex. In this work we analysed only the dependence of V_{rec} with V_A and the turbulence injection parameters. Both, V_{rec} and the acceleration efficiency are clearly dominated by the V_A dependence, as one should expect for any process driving the fast reconnection, though we also obtained some weak dependencies of the acceleration time with the turbulent parameters. For instance, the scattering should happen at scales equal or smaller than l_{inj} , this might be the reason why only the dependence on the injection power and not on injection scale is manifested at lower energies in our results ($E_p < 10^2$, compare Figures 7 and 8). Moreover, at these scales particles can be scattered many times on the same side of the current sheet, with the energy gain temporarily independent of the value of V_{rec} until they are scattered back across the magnetic discontinuity again to complete the first order Fermi cycle.

Having the points above in mind, we should remember that the turbulence is essentially the physical mechanism that drives fast reconnection in the large-scale current sheets studied here. This is a potentially very important driving mechanism because turbulence is very common in astrophysical sources and environments. Nevertheless, the first order Fermi could in principle operate in current sheets with fast reconnection driven by other possible processes and the results should not differ substantially from the present ones. This is compatible with the results found above that show only a weak dependence of the acceleration rate with the parameters of the turbulence. This may also explain why our results are similar to those of kinetic PIC simulations, where the driving mechanisms of fast reconnection are generally very distinct.

It should be also stressed that the collisional MHD simulations shown here focussed on proton acceleration. Although applicable to electrons too, the numerical integration of the electron trajectories is much longer in MHD domains with test particles. Nevertheless, such tests are also needed. Hybrid simulations combining both the PIC and the MHD approach may be a good approach to this problem (e.g., Bai et al. 2015).

We further remark that we have tried to establish a link with the results of the PIC studies which probe only the kinetic scales up to 1000 skin depth scales. But in our collisional study only the injected particles with Larmor radii near the MHD scales are effectively accelerated. This limitation can be also solved using hybrid codes able to resolve both the kinetic and the MHD scales and make a smooth transition between them (de Gouveia Dal Pino & Kowal 2015).

Another note is in order. This work should be distinguished from studies that examined particle acceleration in pure turbulent environments (which are not embedded in large-scale current sheets, see e.g., Dmitruk & Matthaeus 2003; Zharkova et al. 2011; Dalena et al. 2014; Kowal, de Gouveia Dal Pino, & Lazarian 2012; de Gouveia Dal Pino & Kowal 2015).

⁹ It should be stressed that, as in our model, the Fermi acceleration and resulting particle power-law spectrum obtained by Guo et al. (2014, 2015); Li et al. (2015) is due to the electric field produced by the magnetic fluctuations ($-\mathbf{u} \times \mathbf{B}$), while in the case of Sironi & Spitkovsky (2014), it is argued that the acceleration is dominated by the resistive electric field component, which in our case is absent (see also Kowal, de Gouveia Dal Pino, & Lazarian 2012).

Brunetti & Lazarian 2016). For instance, Kowal, de Gouveia Dal Pino, & Lazarian (2012) have compared the two cases and concluded that in the cases with pure turbulence particle acceleration is probably dominated by a second order Fermi process, but further studies must be carried out in order to disentangle the processes.

Finally, cosmic-ray acceleration investigation in magnetic reconnection sites has still many challenges to overcome, particularly in collisional MHD and relativistic regimes. The present study has tried to advance a little in the first of these topics. With regard to the second one, i.e., the study of acceleration in relativistic domains of reconnection, there has been some recent advances both in collisionless descriptions (e.g., Cerutti et al. 2013; Sironi & Spitkovsky 2014; Guo et al. 2014, 2015, and references therein), and in collisional relativistic MHD fast reconnection involving turbulence (e.g., de Gouveia Dal Pino & Kowal 2015; Lazarian et al. 2016; Singh, Mizuno, & de Gouveia Dal Pino 2016; Takamoto, Inoue, & Lazarian 2015; see also de Gouveia Dal Pino, Kowal, & Lazarian 2014 for a short review of both approaches). These are important issues to be explored further, specially for building more realistic models of flares and variability in the spectrum of compact sources to help in the interpretation of current high energy observations and in making predictions for upcoming new generation of instruments, like the Cherenkov Telescope Array (Actis et al. 2011; Acharya et al. 2013; Sol et al. 2013) and the ASTRI CTA Mini-Array (Vercellone 2016).

ACKNOWLEDGEMENTS

M. V. d.V. acknowledges CNPq/Twas for financial support. E.M.G.D.P. acknowledges partial support from the Brazilian agencies FAPESP (grant no. 2013/10559-5 and CNPq (grant no. 300083/94-7). G.K. acknowledges support from FAPESP (grants no. 2013/04073-2 and 2013/18815-0) and PNPd/CAPEs (grant no. 1475088). M. V. d.V. thanks Reinaldo Santos-Lima for fruitful discussions on different topics addressed in this paper. The authors also acknowledge the anonymous referee for a careful review. This work has made use of the computing facilities of the Laboratory of Astroinformatics (IAG/USP, NAT/Unicsul), whose purchase was made possible by the Brazilian agency FAPESP (grant 2009/54006-4) and the INCT-A. M. V. d.V. thanks the great hospitality of the Instituto de Astronomia, Geofísica e Ciências Atmosféricas (São Paulo University), where part of this work was developed.

REFERENCES

Acharya B. S., et al., 2013, *Aph*, 43, 3
 Actis M., et al., 2011, *ExA*, 32, 193
 Alvelius K., 1999, *PhFl*, 11, 1880
 Bai X.-N., Caprioli D., Sironi L., Spitkovsky A., 2015, *ApJ*, 809, 55
 Barres de Almeida U., de Gouveia Dal Pino E. M., 2014, *RMxAC*, 44, 122
 Biskamp D., 1997, *noma.book*, 392
 Brunetti G., Lazarian A., 2016, *MNRAS*, 458, 2584

Cerutti B., Werner G. R., Uzdensky D. A., Begelman M. C., 2014, *ApJ*, 782, 104
 Cerutti B., Werner G. R., Uzdensky D. A., Begelman M. C., 2013, *ApJ*, 770, 147
 Clausen-Brown E., Lyutikov M., 2012, *MNRAS*, 426, 1374
 Dalena S., Rappazzo A. F., Dmitruk P., Greco A., Matthaeus W. H., 2014, *ApJ*, 783, 143
 de Gouveia Dal Pino E. M., Kowal G., Lazarian A., 2014, *ASPC*, 488, 8
 de Gouveia dal Pino E. M., Lazarian A., 2005, *A&A*, 441, 845 (GL05)
 de Gouveia Dal Pino E. M., Piovezan P. P., Kadowaki L. H. S., 2010, *A&A*, 518, A5
 de Gouveia Dal Pino E. M., Kowal G., 2015, *ASSL*, 407, 373
 de Gouveia Dal Pino E. M., Lazarian A., 2001, *ApJ*, 560, 358
 de Gouveia Dal Pino E. M., Lazarian A., 2000, *ApJ*, 536, L31
 de Gouveia Dal Pino E. M., Piovezan P., Kadowaki L., Kowal G., Lazarian A., 2010, *HiA*, 15, 247
 del Valle M. V., Romero G. E., Luque-Escamilla P. L., Martí J., Ramón Sánchez-Sutil J., 2011, *ApJ*, 738, 115
 Dmitruk P., Matthaeus W. H., 2003, *ApJ*, 597, 1097
 Drake J. F., Cassak P. A., Shay M. A., Swisdak M., Quataert E., 2009, *ApJ*, 700, L16
 Drake J. F., Opher M., Swisdak M., Chamoun J. N., 2010, *ApJ*, 709, 963
 Drake J. F., Swisdak M., Che H., Shay M. A., 2006, *Natur*, 443, 553
 Drake J. F., Swisdak M., Fermo R., 2013, *ApJ*, 763, L5
 Drury L. O., 2012, *MNRAS*, 422, 2474
 Eyink G. L., Lazarian A., Vishniac E. T., 2011, *ApJ*, 743, 51
 Giannios D., 2010, *MNRAS*, 408, L46
 Gordovskyy M., Browning P. K., Vekstein G. E., 2010, *ApJ*, 720, 1603
 Gordovskyy M., Browning P. K., 2011, *ApJ*, 729, 101
 Guo F., Li H., Daughton W., Li X., Liu Y.-H., 2016, *PhPl*, 23, 055708
 Guo F., Li H., Daughton W., Liu Y.-H., 2014, *PhRvL*, 113, 155005
 Guo F., Liu Y.-H., Daughton W., Li H., 2015, *ApJ*, 806, 167
 Kadowaki L. H. S., de Gouveia Dal Pino E. M., Singh C. B., 2015, *ApJ*, 802, 113
 Khiali B., de Gouveia Dal Pino E. M., 2016, *MNRAS*, 455, 838
 Khiali B., de Gouveia Dal Pino E. M., del Valle M. V., 2015, *MNRAS*, 449, 34
 Khiali B., de Gouveia Dal Pino E. M., Sol H., 2015, *arXiv*, arXiv:1504.07592
 Kobak T., Ostrowski M., 2000, *MNRAS*, 317, 973
 Kotera K., Olinto A. V., 2011, *ARA&A*, 49, 119
 Kowal G., Lazarian A., Vishniac E. T., Otmianowska-Mazur K., 2012b, *NPGeo*, 19, 297
 Kowal G., de Gouveia Dal Pino E. M., Lazarian A., 2011, *ApJ*, 735, 102
 Kowal G., de Gouveia Dal Pino E. M., Lazarian A., 2012a, *PhRvL*, 108, 241102
 Kowal G., Lazarian A., Vishniac E. T., Otmianowska-Mazur K., 2009, *ApJ*, 700, 63
 Lazarian A., 2005, *AIPC*, 784, 42
 Lazarian A., Desiati P., 2010, *ApJ*, 722, 188
 Lazarian A., Eyink G., Vishniac E., Kowal G., 2014, *ASPC*, 488, 23
 Lazarian A., Kowal G., Takamoto M., de Gouveia Dal Pino E. M., Cho J., 2016, *ASSL*, 427, 409
 Lazarian A., Opher M., 2009, *ApJ*, 703, 8
 Lazarian A., Petrosian V., Yan H., Cho J., 2003, *astro*, arXiv:astro-ph/0301181
 Lazarian A., Vishniac E. T., 1999, *ApJ*, 517, 700
 Lazarian A., Vlahos L., Kowal G., Yan H., Beresnyak A., de Gouveia Dal Pino E. M., 2012, *SSRv*, 173, 557
 Lehe R., Parrish I. J., Quataert E., 2009, *ApJ*, 707, 404

- Li X., Guo F., Li H., Li G., 2015, *ApJ*, 811, L24
Loureiro N. F., Schekochihin A. A., Cowley S. C., 2007, *PhPl*, 14, 100703
Lyubarsky Y., Liverts M., 2008, *ApJ*, 682, 1436-1442
Parker E. N., 1979, *cmft.book*,
Shibata K., Tanuma S., 2001, *EP&S*, 53, 473
Singh C. B., de Gouveia Dal Pino E. M., Kadowaki L. H. S., 2015, *ApJ*, 799, L20
Singh C. B., Mizuno Y., de Gouveia Dal Pino E. M., 2016, *ApJ*, 824, 48
Sironi L., Spitkovsky A., 2014, *ApJ*, 783, L21
Sol H., et al., 2013, *APh*, 43, 215
Takamoto M., Inoue T., Lazarian A., 2015, *ApJ*, 815, 16
Uzdensky D. A., 2011, *SSRv*, 160, 45
Vercellone S., 2016, *EPJWC*, 121, 04006
Vieyro F. L., Romero G. E., 2012, *A&A*, 542, A7
Zenitani S., Hoshino M., 2008, *ApJ*, 677, 530-544
Zenitani S., Hoshino M., 2007, *ApJ*, 670, 702
Zenitani S., Hoshino M., 2001, *ApJ*, 562, L63
Zenitani S., Hesse M., Klimas A., 2009, *ApJ*, 696, 1385
Zhang B., Yan H., 2011, *ApJ*, 726, 90
Zharkova V. V., et al., 2011, *SSRv*, 159, 357

This paper has been typeset from a $\text{\TeX}/\text{\LaTeX}$ file prepared by the author.